ISSN : 1226-7244 (Print)
ISSN : 2288-243X (Online)
논문번호 20-04-09
62

j.inst.Korean.electr.electron.eng.Vol.24,No.4,982~990,December 2020
http://dx.doi.org/10.7471/ikeee.2020.24.4.982

Estimating aquifer location using deep neural network with electrical impedance tomography

Sunam Kumar Sharma*, Anil Kumar Khambampati*, Kyung Youn Kim*★

Abstract

Groundwater is essential source of the freshwater. Groundwater is stored in the body of the rocks or sediments, called aquifer. Finding an aquifer is a very important part of the geophysical survey. The best method to find the aquifer is to make a borehole. Single borehole is not a suitable method if the aquifer is not located in the borehole drilled area. To overcome this problem, a cross borehole method is used. Using a cross borehole method, we can estimate aquifer location more precisely. Electrical impedance tomography is use to estimate the aquifer location inside the subsurface using the cross borehole method. Electrodes are placed inside each boreholes and area between these boreholes are analysed. An aquifer is a non-uniform structure with complex shape which can represented by the truncated Fourier series. Deep neural network is evaluated as an inverse problem solver for estimating the aquifer boundary coefficients.

Key words : Deep neural network, electrical impedance tomography, aquifer, estimation, inverse problem, Fourier coefficient

Ⅰ. Introduction

Fresh water is the most crucial item for human being and hydrological cycle of the earth [1][2]. Fresh water includes water in ice caps, glaciers, ponds, lakes, river, groundwater, etc, [3]. Groundwater is stored in the body of a rock or sediments known as an aquifer [4][5]. This makes the exploration of aquifer most important task in the geophysical survey. To find the location of an aquifer traditionally a borehole method is used. In this method a hole is made in the ground and samples are collected at certain levels to determine the existence of an aquifer. This method is time consuming, and if the aquifer is not located in the position of the hole, the aquifer is not identified.

Geophysics survey can be done based on the electro-magnetic property of materials. Magnetic resonance tomography generates images based on the magnetic distribution properties of the subsurface [6]. For data acquisition a huge magnetic coil is hanged from the helicopter and the data is collected, which is a huge task and the implementation cost is very high [7]. On the other hand, implementation of electrical impedance tomography is very easy and low cost compare to magnetic resonance tomography. Electrical impedance tomography (EIT) generates cross-sectional images of the conductivity distribution

* Department of Electronic Engineering, Jeju National University
★ Corresponding author
email: kyungyk@jejunu.ac.kr, Tel : +82-64-754-3664
※ Acknowledgment
Manuscript received Nov. 24, 2020; revised Dec. 13, 2020; Dec. 15, accepted 2020.

of the object [8]. EIT have been used to study subsurface pollutant [9], petroleum reservoir monitoring [10], process flow monitoring [11], and also in medical applications [12-15]. The surface electrode method is good for the case where an aquifer is located near the surface, but if an aquifer is deeper than this method is not suitable. For deeper layer estimation cross borehole method is used [16]. In the cross borehole method, electrodes are placed inside the borehole at equidistance in each hole. EIT generated the cross sectional image of the subsurface located between the two boreholes based on the measured voltage data. This image represents the conductivity distribution of the subsurface.

Most of the studies in EIT have estimated the pixel conductivity, but they are affected by poor spatial resolution [17]. Due to the poor spatial resolution the boundaries of the aquifer is not properly generated. The shape estimation approach can improve the spatial resolution [18]. When estimating the shape coefficients in the complex domain higher order Fourier coefficients are used. Normal optimization algorithm such as mNR algorithm tends to have intersecting boundaries while estimating the shape coefficients due to the presence of Jacobian matrix [19].

Over the past few years, neural network algorithm have been implemented for solving the complex problems. In [20] authors have implemented deep neural network as an inverse problem solver for estimating the bladder boundary and has evaluated that mNR algorithm fails to predict high-order Fourier coefficients for complex shapes. The neural network algorithm does not need a Jacobian matrix and can be used as a shape coefficient estimator. Neural network algorithm maps the measured voltage data with the Fourier series shape coefficients.

In this work, a deep neural network [21] algorithm is proposed as an inverse problem solver for estimating Fourier coefficients which defines the shape and location of the aquifer between the boreholes. The schematic diagram for the cross borehole system used in this work is shown in figure 1. From the figure we can see that the electrodes are located on the surface of the domain under analysis. These electrodes are placed inside the borehole at a predefined depth. We have implemented the 6-layer neural network for the image reconstruction estimating the boundary of the aquifer in EIT. The algorithm has been trained with the simulated data which consists of boundary voltage measurement and the corresponding Fourier coefficients. The background different layers are considered to be alluvium and clay. To evaluate the algorithm, unseen data of boundary voltage measured across the cross borehole electrodes on the subsurface domain were used. Numerical simulations were performed for the evaluation of the proposed method.

II. Electrical Impedance Tomography

Electrical impedance tomography (EIT) reconstruct the conductivity distribution of object. To reconstruct an image of an aquifer inside the subsurface domain between the cross borehole as shown in figure 1. A small magnitude of current $I_l(l=1,2,\cdots,L)$ is injected through electrodes $e_l(l=1,2,\cdots,L)$ which is placed inside the cross borehole along the surface $\partial\Omega$ of the subsurface domain. Let conductivity distribution of domain be $\sigma(x,y)$ and the resultant measured voltages be $u(x,y)$ across the electrodes. The relationship between conductivity distribution and the measured voltages are described by Maxwell equation of electromagnetism as [22][23].

$$\nabla\cdot(\nabla\sigma u(x,y))=0,(x,y)\in\Omega \quad (1)$$

In EIT, complete electrode model (CEM) is used as it is more realistic and accurate model [24]. Kirchhoff's laws on the measured voltages and injected currents are needed for the uniqueness and the existence of the solution [25]. The reconstruction procedure of an image in EIT consists of the forward and inverse problem.

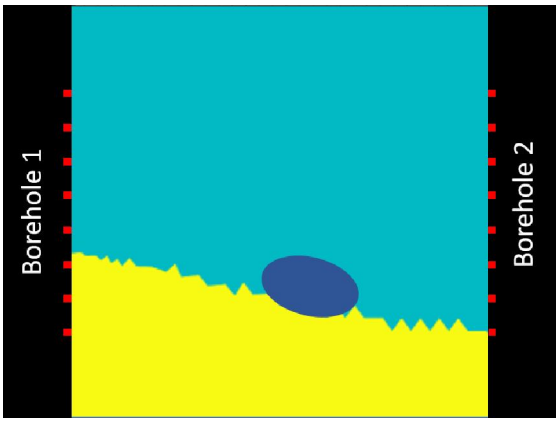

Fig. 1. Schematic diagram of the subsurface domain. Electrodes (shown in red colour) are placed inside borehole along the boundary of the domain.

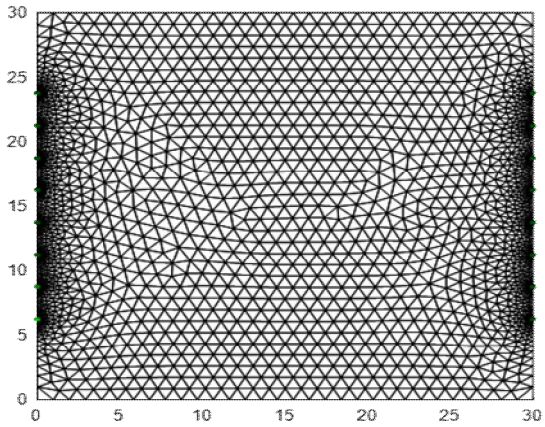

Fig. 2. Domain mesh generated using a finite element method (FEM).

1. Forward Problem

Calculation of the measured boundary voltage across the surface electrodes using known internal conductivity distribution of subsurface domain and injected currents falls in the forward problem. In this work finite element method (FEM) [26] have been used to address the forward problem. The subsurface domain Ω is discretized into small triangular elements as shown in figure 2. In FEM, electrical potential u and the conductivity distribution σ within the subsurface domain are approximated as u^h and σ^h, are assumed to be uniform within each element and is represented as

$$u(x,y) \approx u^h(x,y) = \sum_{i=1}^{N_n} \alpha_i \phi_i(x,y) \tag{2}$$

$$\sigma(x,y) \approx \sigma^h(x,y) = \sum_{i=1}^{N_e} \sigma_i \psi_i(x,y) \tag{3}$$

where ϕ_i, ψ_i are the two-dimensional first-order basis functions for electrical potential and resistivity distribution and α_i is the voltage to be determined. N_n and N_e are the number of nodes and elements in domain mesh. The voltage U on electrodes are approximate as

$$U \approx U^h = \sum_{j=1}^{L-1} \beta_j \eta_j \tag{4}$$

where β_j are voltages to be determine. $\eta_1 = (1,-1,0,\cdots,0)^T$, $\eta_2 = (1,0,-1,0,\cdots,0)^T \in R^{L\times 1}$ are the bases for the measurement. The finite element formulation can be expressed as a set of linear equations

$$Ab = f \tag{5}$$

where A is the stiffness matrix, f is current vector and b is nodal boundary voltage vector. For more details regarding FEM formulation, refer to [27]. The forward solution is computed using EIDORS [28] in MATLAB.

2. Parameterization of aquifer boundary

Let us assume a closed and disjoint known region with a smooth boundary $\partial\Omega$ in the domain Ω. The truncated fourier series approach can be used to approximate the boundaries inside the region as [29].

$$B_n(s) = \begin{pmatrix} x_n(s) \\ y_n(s) \end{pmatrix} = \sum_{f=1}^{F_\Lambda} \begin{pmatrix} \lambda_f^{x_n} \Phi_f^{x_n}(s) \\ \lambda_f^{y_n} \Phi_f^{y_n}(s) \end{pmatrix} \tag{6}$$

where $n = (1,2,\cdots,S)$, $B_n(s)$ is the boundary of the nth object, S is the number of disjoint objects in the domain Ω, F_Λ is the order of the truncated Fourier series and $\Phi_f(s)$ is the basis function which is periodic.

Using the above basis function in equation (6),

the aquifer boundary $B_n(s)$ can be expressed as Y shape coefficients represented as

$$Y=(\lambda_1^{\mu_1},\cdots,\lambda_{F_A}^{\mu_1},\lambda_1^{\mu_s},\cdots,\lambda_{F_A}^{\mu_s})^T \tag{7}$$

Y is estimated using a deep neural network algorithm.

3. Inverse solver

Measured boundary voltages and the applied currents through the cross borehole electrodes located on the boundary of the domain are used to estimate the conductivity distribution of the domain. The inverse problem in EIT can be a shape estimation problem, if the conductivity values of the region can be known as a priori and object boundary is inside the domain.

We have used deep neural network algorithm as an inverse solver to estimate the aquifer boundary. Measured boundary voltages are used as an input for Deep neural networks (DNN) which maps the non-linear relationship between input voltage data and Fourier coefficient. DNN has six layers i.e. input layer, output layers and 4 hidden layers between input and output layers which can be seen in the schematic diagram of the model in figure 3.

The boundary voltage data is used as input which makes the neurons of the input layer. The neurons of the output layer represents the Fourier coefficients. The hidden layers is used as a relationship mapping between input and output layers.

A dataset containing measured boundary voltages and the corresponding Fourier coefficients is used. The dataset is separated as training and testing dataset. The testing data dataset is used to evaluate the model and the training dataset is used to learn the relationship between measured voltages and Fourier coefficients using a mapping function $H_\theta(\nu)$ and expressed as

$$H_\theta(\nu)=\sum_{k=0}^{m}\theta^k\nu^k=\theta^T\nu \tag{8}$$

where θ is the weight. The Rectified linear unit (ReLU) [30] have been used as an activation function which is defined as

$$f(\nu)=\max(0,\nu) \tag{9}$$

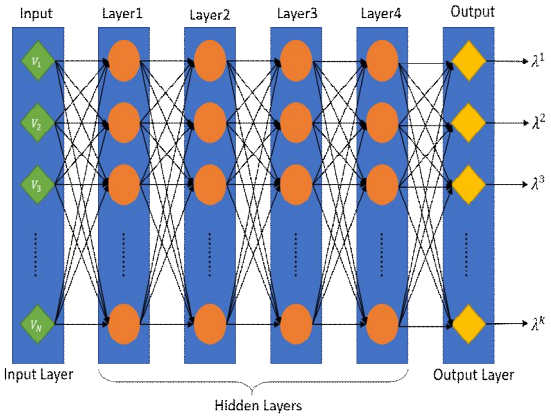

Fig. 3. Schematic diagram of deep neural network. Voltage data is used as input in input layer and Fourier coefficients is the output of output layers. Four hidden layers in between input and output layers.

The weights θ of the nodes are estimated by minimizing the cost function using deep neural network. Cost function is defined as the sum of the error between the estimated output and the desired output value. The cost function is defined as

$$\gamma=\frac{1}{m}\sum_{k=1}^{m}(H(\nu^k)-\lambda^k)^2 \tag{10}$$

where $H(\nu^k)$ is the DNN predicted output and λ^k is the desired output at k^{th} sample. To determine the weight θ, we minimize the least square cost function as

$$\theta=\arg_\theta\min\sum_{k=1}^{m}\parallel H(\nu^k)-\lambda^k\parallel^2 \tag{11}$$

here m is the number of training dataset for the model. For computing the weights in the deep neural network model with minimization of the cost function $\gamma(\theta)$ adam's optimization [31] is used. Adam's optimization update the weights θ as

$$\theta_{t+1} = \theta_t - \alpha \frac{d\gamma(\theta)}{\sqrt{o_t} + \epsilon} \quad (12)$$

where, $o_t = \beta_2 o_{t-1} + (1-\beta_2) d\gamma(\theta)_t^2$, α is learning rate, β_2 is the hyper parameter, and ϵ is a small value.

III. Results and discussions

The visualization of aquifer boundary estimation in the subsurface domain using deep neural network (DNN) is presented in this section. To estimate the boundary of aquifer, which is located in the background having two different conductivities, DNN was used. The data for training the DNN is generated using EIDORS. The dimension of the domain taken is 30m by 30m. A finite element subsurface domain with 10968 triangular elements and 5781 nodes are used for generating simulated voltage data for different aquifer sizes during the generation of training and testing data.

To represent the shape of the aquifer inside the domain, truncated Fourier series is used. A complex shaped of the aquifer boundary was described by the total of six Fourier coefficients. The electrical conductivities of two different backgrounds (alluvium and clay) and aquifer are considered as 0.004S/m, 0.321S/m, and 0.066S/m, respectively [32]. Using the attached 16 surface electrodes, 10 mA magnitude of current is injected using the adjacent injection pattern.

A 6-layer deep neural network was designed which consists of one input layer, 4 hidden layers, and one output layer as shown in figure 3. Number of nodes in the input layer is 256, in the output layer is 6, and in 4 hidden layers are 256, 64, 128, 64, respectively.

The number of nodes in hidden layers used are the result of hyper-parameter tuning of the model. Different numbers of hidden layers were used and analysed. Different number of hidden layers are used during development of the model. The simplest model had 2 hidden layers and the most complex model had 5 hidden layers. The model which was more generalized towards the validation dataset and had low training loss was chosen as the appropriate model. From the table 1 we can see that the model with the 5 number of hidden layers has the lowest training loss, however the validation loss is higher than the 4 hidden layers model. The model with 5 hidden layers seems to be overfitting. Model with 4 hidden layers has very less difference between the training loss and validation loss which is suitable for the definition of generalized model. Thus model with 4 hidden layers is used in this work.

Table 1. Training and validation loss of the DNN with different number of hidden layers.

No. of hidden layers	Training loss	Validation loss
2	11.279	14.465
3	7.7766	12.8065
4	3.5667	3.6737
5	2.5498	3.7690

The DNN model is trained and tested using 10 thousand pairs of simulated data (measured boundary voltage and corresponding Fourier coefficients). DNN algorithm was implemented in python using TensorFlow library [33] with mean square error (MSE) as loss function and Adam optimizer as optimization function. Workstation used for training and testing of DNN model has a configuration of Intel(R) Core(TM) i7-6700 CPU @ 3.40GHz, 8GB RAM, NIVIDIA GeForce GT730 GPU, Windows 10. The DNN model was trained with 1500 epochs with batch size 8 per epoch. 20% of the training dataset was separated for the validation of the model. The learning rate of Adam was set to 1e-3.

Training loss and validation loss per epoch is plotted in figure 4. From the figure we can see that the model loss is decreasing to a significant level which allows for the prediction of the

Fourier coefficients with good accuracy. The figure shows the validation loss is higher than the training loss because the model is being validated with unseen data.

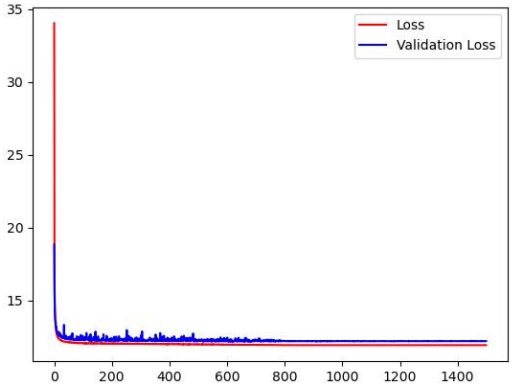

Fig. 4. Training loss and validation loss of the DNN model using the training process. Red is the training loss and blue is the validation loss per epoch.

The aquifer location in the subsurface domain between the boreholes is plotted in figure 5 as case 1. In this case, the aquifer is assumed to be small in size. The blue coloured background is assumed to be alluvium and yellow coloured background is assumed to be clay. Figure 6 shows the reconstructed image of the aquifer boundary along with the background for the case 1. As conductivities of target and backgrounds are assumed to be known as priori. The estimated boundary coefficients of the aquifer by DNN has a good accuracy.

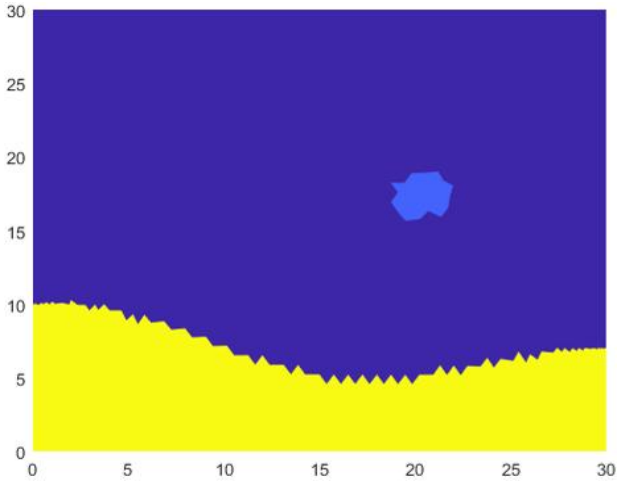

Fig. 6. Reconstructed image of the aquifer for case1 with the background inside the subsurface domain. Light blue coloured target is the estimated aquifer by DNN method.

Figure 7 shows the case 2 of the aquifer location. In this case an aquifer has bigger size than the case 1. Figure 8 shows the reconstructed image of the aquifer boundary for the case 2 along with the background. DNN estimated result has the good accuracy of an aquifer boundary located inside the domain.

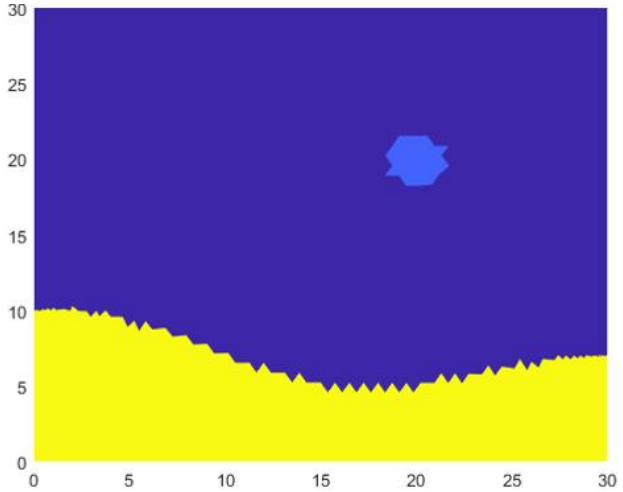

Fig. 5. True image of the aquifer with the background of known conductivity for case1. The light blue coloured target is the aquifer in assume background of alluvium and clay.

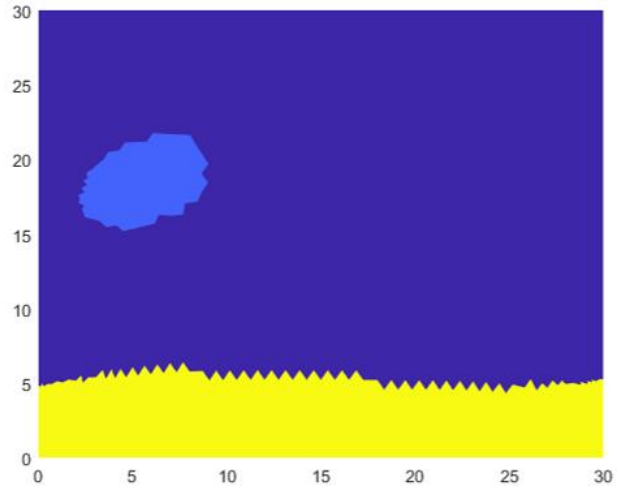

Fig. 7. True image of the aquifer with the background of known conductivity for case2. The light blue coloured target is the aquifer in assume background of alluvium and clay.

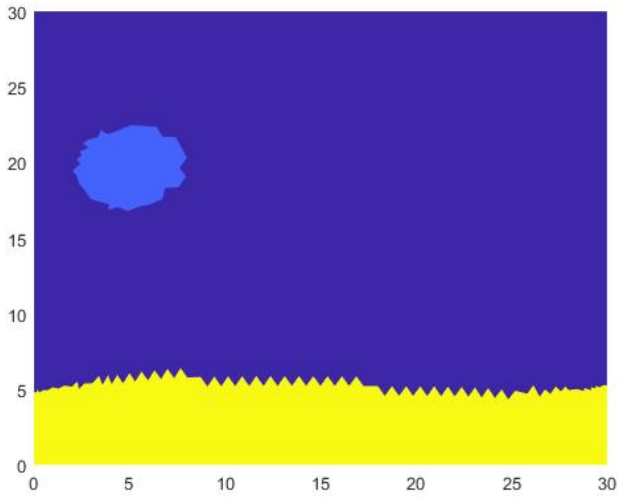

Fig. 8. Reconstructed image of the aquifer for case2 with the background inside the subsurface domain. Light blue coloured target is the estimated aquifer by DNN method.

To evaluate the accuracy for the estimated aquifer boundary coefficients root mean square error (RMSE) is used. The RMSE for the estimated aquifer boundary coefficient is defined as

$$error_{\lambda} = \sqrt{\frac{(\lambda-\lambda_{true})^{T}(\lambda-\lambda_{true})}{\lambda^{T_{true}}\lambda_{true}}} \qquad (13)$$

where λ is estimated Fourier coefficients and λ_{true} is the true Fourier coefficients. Table 2 shows the RMSE values of both cases.

Table 2. RMSE values for cases estimated by DNN.

Case	RMSE
1	0.0937
2	0.1483

III. Conclusions

The estimation of aquifer boundary inside the subsurface domain using electrical impedance tomography was studied. An aquifer boundary inside the subsurface domain have been approximated by the truncated Fourier series. Since the electrical conductivities of the backgrounds and the aquifer are known a priori. A six layered deep neural network algorithm is designed to estimate the target aquifer boundary. Deep neural network has been trained and evaluated with the measured boundary voltage and corresponding Fourier coefficients of aquifer boundary. The evaluation data was never used with the testing data. The estimated boundary of the aquifer by the proposed DNN had a reasonable accuracy. Also, DNN do not require any initial guess and Jacobian matrix computations.

References

[1] E. Custodio, “Aquifer overexploitation: what does it mean?,” *Hydrogeology journal* vol.10, no.2, pp.254-277, 2002.
DOI: 10.1007/s10040-002-0188-6

[2] A. Pidlisecky, T. Moran, B. Hansen and R. Knight, “Electrical resistivity imaging of seawater intrusion into the Monterey Bay aquifer system,” *Groundwater,* vol.54, no.2, pp.255-261, 2016.
DOI: 10.1111/gwat.12351

[3] S. L. Postel, G. C. Daily and P. R. Ehrlich, “Human appropriation of renewable fresh water,” *Science,* vol.271, no.5250, pp.785-788, 1996.
DOI: 10.1126/science.271.5250.785

[4] P. H. Gleick and N. L. Cain, *The world’s water 2004~2005: the biennial report on freshwater resources.* Island Press, 2004.

[5] D. M. Bonotto, “Natural radionuclides in major aquifer systems of the Paraná sedimentary basin, Brazil,” *Applied Radiation and Isotopes*, vol.69, no.10, pp.1572-1584, 2011.
DOI: 10.1016/j.apradiso.2011.06.002

[6] S. Okuma, T. Nakatsuka, M. Komazawa, M. Sugihara, S. Nakano, R. Furukawa, R. Supper, “Shallow subsurface structure of the Vulcano-Lipari volcanic complex, Italy, constrained by helicopter-borne aeromagnetic surveys,” *Exploration Geophysics,* vol.37, no.1, pp.129-138, 2006.
DOI: 10.1071/EG06129

[7] K. Okazaki, T. Mogi, M. Utsugi, Y. Ito, H. Kunishima, T. Yamazaki, & H. Kaieda, “Airborne

electromagnetic and magnetic surveys for long tunnel construction design." *Physics and Chemistry of the Earth, Parts A/B/C*, vol.36, no.16, pp. 1237-1246, 2011. DOI: 10.1016/j.pce.2011.05.008

[8] M. Cheney, D. Isaacson, and J. C. Newell, "Electrical impedance tomography," *SIAM review,* vol.41, no.1, pp.85-101, 1999.

[9] G. D'Antona, A. Ferrero, M. Lazzaroni, R. Ottoboni, and E. Samarani, "Active monitoring apparatus for underground pollutant detection based on electrical impedance tomography," *Proceedings of the 19th IEEE Instrumentation and Measurement Technology Conference* (IEEE Cat. No. 00CH37276), vol.1, pp.577-579, 2002. DOI: 10.1109/IMTC.2002.1006906

[10] R. Stacey, K. Li, R. N. Horne, "Electrical impedance tomography (eit) technique for real-time saturation monitoring," in *SPE Annual Technical Conference and Exhibition, Society of Petroleum Engineers*, 2006.

[11] A. K. Khambampati, B. A. Lee, K. Y. Kim, and S. Kim, "An analytical boundary element integral approach to track the boundary of a moving cavity using electrical impedance tomography," *Measurement Science and Technology*, vol.23, no.3, pp.035401, 2012. DOI: 10.1088/0957-0233/23/3/035401

[12] A. Adler, J. H. Arnold, R. Bayford, A. Borsic, B. Brown, P. Dixon, T. J. Faes, I. Frerichs, H. Gagnon, Y. Garber, et al., "Greit: a unified approach to 2d linear eit reconstruction of lung images," *Physiological measurement*, vol.30, no.6, p.S35, 2009. DOI: 10.1088/0967-3334/30/6/S03

[13] D. Holder, "Electrical impedance tomography (eit) of brain function," *Brain Topography*, vol.5, no.2, pp.87-93, 1992. DOI: 10.1007/BF01129035

[14] E. K. Murphy, A. Mahara, X. Wu, and R. J. Halter, "Phantom experiments using soft-prior regularization eit for breast cancer imaging," *Physiological measurement*, vol.38, no.6, pp.1262, 2017. DOI: 10.1088/1361-6579/aa691b.

[15] S. K. Sharma, S. K. Konki, A. K. Khambampati, and K.Y. Kim, "Bladder boundary estimation by Gravitational Search Algorithm using Electrical Impedance Tomography," I*EEE Transactions on Instrumentation and Measurement,* vol.69, no.12, pp.9657-9667, 2020. DOI: 10.1109/TIM.2020.3006326

[16] W. Menke, "The resolving power of cross borehole tomography," *Geophysical Research Letters*, vol.11, no.2, pp.105-108, 1984. DOI: 10.1029/GL011i002p00105

[17] D. Liu, Y. Zhao, A. K. Khambampati, A. Seppanen, and J. Du, "A parametric level set method for imaging multiphase conductivity using electrical impedance tomography," *IEEE Transactions on Computational Imaging*, vol.4, no.4, pp.552-561, 2018. DOI: 10.1109/TCI.2018.2863038

[18] M. C. Kim, K. Y. Kim, and S. Kim, "Estimation of phase boundaries in two-phase systems by an electrical impedance tomography technique," *Journal of Industrial and Engineering Chemistry*, vol.10, no.5, pp.710-716, 2004. DOI: 10.3811/jjmf.24.435

[19] B. Brandstatter, "Jacobian calculation for electrical impedance tomography based on the reciprocity principle," *IEEE transactions on magnetics*, vol.39, no.3, pp.1309-1312, 2003. DOI: 10.1109/TMAG.2003.810390

[20] S. K. Konki, A. K. Khambampati, S. K. Sharma, and K. Y. Kim, "Deep neural network for estimating the bladder boundary using electrical impedance tomography," *Physiological Measurement,* 2020.

[21] W. Liu, Z. Wang, X. Liu, N. Zeng, Y. Liu, and F. E. Alsaadi, "A survey of deep neural network architectures and their applications," *Neurocomputing*, vol.234, pp.11-26, 2017.

[22] D. Holder, *Electrical impedance tomography: methods, history and applications*. CRC Press, 2004.

[23] D. L. Colton, R.E. Ewing, and W. Rundell, eds., *Inverse problems in partial differential equations (Vol. 42),* Siam, 1990.

[24] K. S. Cheng, D. Isaacson, J. C. Newell, and D. G. Gisser, "Electrode models for electric current

computed tomography." *IEEE Transactions on Biomedical Engineering*, vol.36, no.9, pp.918-924, 1989.
[25] E. Somersalo, M. Cheney, and D. Isaacson, "Existence and uniqueness for electrode models for electric current computed tomography." *SIAM Journal on Applied Mathematics*, vol.52, no.4, pp. 1023-1040, 1992.
[26] O. C. Zienkiewicz, *Finite Element Method: Vol. 3: Fluid Dynamics. Vol. 3,* Elsevier Science & Technology Books, 2000.
[27] M. Vauhkonen, D. Vadasz, P. A. Karjalainen, E. Somersalo, and J. P. Kaipio, "Tikhonov regularization and prior information in electrical impedance tomography." *IEEE transactions on medical imaging*, vol.17, no.2, pp.285-293, 1998.
[28] A. Adler and W. R. Lionheart, "Uses and abuses of eidors: an extensible software base for eit," *Physiological measurement*, vol.27, no.5, pp. S25, 2006.
[29] V. Kolehmainen, A. Voutilainen, and J. P. Kaipio, "Estimation of non-stationary region boundaries in eit-state estimation approach," *Inverse Problems*, vol.17, no.6, pp.1937, 2001.
[30] A. F. Agarap, "Deep learning using rectified linear units (relu)." *arXiv preprint arXiv:1803.08375,* 2018.
[31] D. P. Kingma, and J. Ba, "Adam: A method for stochastic optimization." *arXiv preprint arXiv: 1412.6980,* 2014.
[32] R. Saad, M. N. M. Nawawi, and E. T. Mohamad, "Groundwater detection in alluvium using 2-D electrical resistivity tomography (ERT)," *Electronic Journal of Geotechnical Engineering,* vol.17, pp. 369-376, 2012.
[33] M. Abadi, P. Barham, J. Chen, Z. Chen, A. Davis, J. Dean, M. Devin, S. Ghemawat, G. Irving, M. Isard, and M. Kudlur, "Tensorflow: A system for large-scale machine learning," In *12th {USENIX} symposium on operating systems design and implementation ({OSDI} 16),* pp.265-283, 2016.

BIOGRAPHY

Sunam Kumar Sharma (Member)

2006 : BE degree in Electronics and Communication Engineering, Pokhara University, Nepal.
2016 : MS degree in Information Technology, Sikkim Manipal University, India.

Anil Kumar Khambampati (Member)

2003 : BS degree in Mechanical Engineering, Jawaharlal Nehru Technological University, India.
2006 : MS degree in Marine Instrumentation Engineering, Jeju National University.
2010 : PhD degree in Electronic Engineering, Jeju National University.

Kyung Youn Kim (Member)

1983 : BS degree in Electronic Engineering, Kyungpook National University.
1986 : MS degree in Electronic Engineering, Kyungpook National University.
1990 : PhD degree in Electronic Engineering, Kyungpook National University.
1990~Present : Professor, Department of Electronic Engineering, Jeju National University.